HHS Public Access

Author manuscript

J Orthop Res. Author manuscript; available in PMC 2016 March 01.

Published in final edited form as:

J Orthop Res. 2015 March ; 33(3): 366–372. doi:10.1002/jor.22768.

Characterization of Bone Perfusion by Dynamic Contrast-Enhanced Magnetic Resonance Imaging and Positron Emission Tomography in the Dunkin-Hartley Guinea Pig Model of Advanced Osteoarthritis

Jonathan P. Dyke, Ph.D.[1,2], **Michael Synan, B.S.**[2], **Paula Ezell, D.V.M.**[3], **Douglas Ballon, Ph.D.**[1,2], **Jennifer Racine, B.A.**[4], and **Roy K. Aaron, M.D.**[4]

[1]Department of Radiology, Weill Cornell Medical College, New York, NY

[2]Citigroup Biomedical Imaging Center, Weill Cornell Medical College, New York, NY

[3]Department of Comparative Medicine, Medical University of South Carolina, Charleston, SC

[4]Department of Orthopedics, The Warren Alpert Medical School of Brown University, Providence, RI

Abstract

Purpose—This study characterizes changes in subchondral bone circulation in OA and examines relationships to bone structure and cartilage degeneration in Dunkin-Hartley guinea pigs.

Methods—We have used dynamic contrast-enhanced MRI (DCE-MRI) and PET, with pharmacokinetic modeling, to characterize subchondral bone perfusion. Assessments are made of perfusion kinetics and vascular permeability by MRI, and blood volume and flow, and radionuclide incorporation into bone, by PET. These parameters are compared to cartilage lesion severity and bone histomorphometry. Assessments of intraosseous thrombi are made morphologically.

Results—Prolonged signal enhancement during the clearance phase of MRI correlated with OA severity and suggested venous stasis. Vascular permeability was not increased indicating that transvascular migration of contrast agent was not responsible for signal enhancement. Intraosseous thrombi were not observed. Decreased perfusion associated with severe OA was confirmed by PET and was associated with reduced radionuclide incorporation and osteoporosis.

Discussion—MRI and PET can be used to characterize kinetic parameters of circulation in OA and correlate them with subchondral bone metabolism of interest to the pathophysiology of OA. The significance of these observations may lie in alterations induced in the expression of cytokines by OA osteoblasts that are related to bone remodeling and cartilage breakdown.

Keywords

Osteoarthritis; PET; MRI; subchondral bone; perfusion

Corresponding Author: Jonathan P. Dyke, Ph.D., Weill Cornell Medical College, 1300 York Avenue – Box 234, New York, NY 10021, (212) 746-5781 Office, jpd2001@med.cornell.edu.

Introduction

Structural and metabolic changes in subchondral bone may play roles in the pathophysiology of OA and even may precede cartilage degeneration in some models.[1-4]. OA osteoblasts have been shown to alter their expression of growth factors and signaling cytokines, modifying the phenotype of chondrocytes, and degrading OA cartilage matrix.[5; 6] Pathways of communication between subchondral bone and cartilage have been described suggesting mechanisms by which osteoblast-derived cytokines could contribute to articular cartilage breakdown and joint inflammation.[7; 8] These observations collectively suggest that subchondral OA osteoblasts may contribute to the pathophysiology of OA and that the subchondral bone may itself be an appropriate therapeutic target.[1; 4; 9]

Osteoblasts alter their expression of structural and signaling proteins in response to changes in perfusion, fluid flow, and oxygen content.[10; 11] Changes in the circulatory environment of subchondral bone in OA may be well within the range to which osteoblasts are responsive.[12] Venous outflow obstruction, decreased perfusion, hypoxia, and intraosseous hypertension occur in late stage OA but the mechanisms are unknown.[13; 14] We have previously demonstrated that decreased perfusion temporally precedes and spatially localizes with eventual cartilage lesions in young Dunkin-Hartley guinea pigs.[15] We have also shown that similar changes occur in human OA and avascular necrosis.[16] Decreased perfusion of OA subchondral bone may alter the physicochemical environment of osteoblasts sufficiently for them to express different cytokine patterns and alter both structural elements – subchondral bone plate and trabeculae– and signaling cytokines, that contribute to cartilage degradation. The current study was undertaken to further characterize changes in circulation that occur in subchondral bone in OA and to examine the relationship of subchondral bone perfusion to bone structure and cartilage degeneration in OA in older guinea pigs.

DCE-MRI with small molecule (SMCM) and macromolecular (MMCM) contrast media offers the opportunity to extract kinetic information on bone circulation including bone blood flow, capillary permeability, interstitial diffusion and venous outflow.[17; 18] Positron emission tomography (PET) using ^{18}F-Fluoride, provides estimates of bone blood flow and bone formation.[19-22]

Materials and Methods

Animal Procedures

Ten Dunkin-Hartley guinea pigs were studied under protocols approved by the IACUCs of both Rhode Island Hospital (Providence) and Weill Cornell Medical College (New York). Dunkin-Hartley guinea pigs are a well-established model of spontaneous OA resembling human disease. Dunkin-Hartley guinea pigs were acquired from Elm Hill Labs (Chelmsford, MA) and Hilltop Lab Animals, Inc (Scottdale, Pennsylvania). The animals had an average weight of 1.02 ± 0.15 kg and an average age of 21.2 ± 2.9 months. Central jugular venous catheters and vascular access ports were placed for bolus injection of MRI and PET tracers. Animals were sedated and maintained via mask on 2.0%-3.0% isoflurane. Buprenorphine (0.05 mg/kg) was given for analgesia. One knee was imaged for each animal.

DCE-MRI Estimation of Bone Perfusion and Capillary Permeability

SMCM Gadopentetate Dimeglumine (m.w. 530 Daltons) [Gd-DTPA, Magnevist, Berlex Laboratories, Wayne, NJ.] was administered at a dose of 0.3 mmol/kg (0.6 ml/kg). The MMCM Gd-Albumin[35] (m.w. 92,000 Daltons) was given at a dose of 0.03 mmol/kg (1.2 ml/kg) [UCSF, Contrast Media Laboratory, San Francisco, CA]. Imaging of SMCM and MMCM were separated by 24 hours between scans, and imaging of the SMCM was always performed prior to that of the MMCM, to allow for complete clearance of contrast. All studies were performed on a 3.0 Tesla GE HDx MRI Scanner (General Electric; Milwaukee, WI). Animals were placed in a custom-designed apparatus that included a 7-loop, 3.2-cm-diameter inductively coupled solenoidal radiofrequency resonator. The DCE-MRI perfusion sequence was a fast 2D multi-plane spoiled gradient echo sequence with 4-5 slices, using a 256 × 128 matrix, a 12.1/3.8 ms TR/TE and a 20 degree flip angle.

Data was analyzed using previously published in-house software yielding parameters based on the Brix two-compartment model.[23] The region of interest (ROI) was drawn from the subchondral plate to the growth plate and from the midline to the medial or lateral cortex, respectively and was the same for PET and histomorphometry. Signal intensities within the ROI were averaged to generate a time intensity curve (TIC). From the Brix model, three parameters were obtained from the compartmental fit of the TIC within each voxel: A, k^{ep}, and k^{el}.[24] The amplitude, A, is related to the extravascular extracellular space (v^e), while k^{ep} is the ratio of the permeability surface area product (PS) divided by v^e. The elimination rate, k^{el}, describes clearance or washout of the contrast agent from the tissue. The large molecular size of the MMCM allows an accurate estimate of the permeability surface area product because it only diffuses out of pathologic vessels with greatly compromised endothelial permeability while SMCM may also diffuse out of normal vessels.[25] An average plasma curve $C^p(t)$ was used for all animals. The permeability surface area product (PS), blood volume (BV), and plasma volume (PV) were determined graphically with the Patlak method.[25]

PET for the Determination of Blood Volume, Perfusion, and Bone Uptake

^{18}F-Fluoride PET data of guinea pig knees were acquired on a Siemens/CTI Concorde Focus 220 μPET scanner (Siemens Medical; Knoxville, TN). PET imaging utilized a 12.2 cm × 12.2 cm × 7.5 cm field of view with a 128 × 128 × 95 matrix size. ROIs were defined using the central single slice coronal plane defining the medial and lateral tibial plateau. Analysis of ^{18}F-Fluoride PET data was based on the three-compartment model described by Hawkins.[26] An average plasma curve was created and analysis was performed using the PMOD 3.1 package [PMOD Technologies Ltd., Zurich, Switzerland]. ^{18}F-Fluoride PET quantifies a perfusion phase within 2 minutes after bolus injection of the radionuclide, yielding estimates of blood flow (K^1) and volume (V^b) in subchondral bone. ^{18}F-Fluoride estimates of bone blood flow have been validated with ^{15}O-H^2O PET.[27] 45-60 minutes post-injection ^{18}F-Fluoride is incorporated into the hydroxyapatite crystal of the bone to form fluoroapatite.[28] This net uptake of fluoride to the bone mineral compartment, termed the net fluoride influx rate (K^i), is indicative of the extent of bone formation and mineralization.[19-22]

Histology and Histomorphometry

After scanning, knees were removed and OA lesions were identified with India ink. Tibias were fixed in zinc formalin, decalcified, and embedded in paraffin. 5 μm coronal sections were cut through the OA lesion or the middle third of the tibia if no lesions were present. Sections were stained with hematoxylin/Safranin O/fast green for histological-histochemical analysis (Mankin).[29] Quantitative histomorphometry of the subchondral bone carried out with a Nikon Microphot FXA light microscope at 25x magnification with Bioquant Osteo II program (Bioquant, Nashville, TN). Subchondral vessels were studied for the presence of thrombi with Martius Blue histochemistry and thrombomodulin immunohistochemistry. Immunohistochemical staining for endothelial thrombomodulin is a marker of endothelial injury and decreased staining is associated with thrombosis. An antigen retrieval procedure was done by incubating with pepsin (ThermoFisher Scientific) and staining was accomplished using the Dako EnVision +System-HRP kit # K4007 (Dako, Carpenteria, CA). After blocking non-specific binding, slides were incubated with primary anti-thrombomodulin mouse monoclonal antibody HRP labeled goat anti-mouse immunoglobulin.

Statistical Methods

Results are expressed as the mean and standard error of the mean (SEM) and compared for significance. Comparisons were made between the MRI and PET derived imaging parameters and the histologically determined Mankin scores. Simple linear regression using ordinary least squares techniques were used to calculate a linear regression between dependent and independent variables. The squared Pearson product moment correlation coefficient (R^2) was then calculated to assess the goodness of fit of the regression. Parametric data was assessed for significance by 2-tailed Students' t-test. Results were considered statistically significant when $p<0.05$.

Results

OA lesions occurred in the medial tibio-femoral compartment. The severity of OA was assessed by histological-histochemical scores (Mankin) and ranged from 0-14 in animals of similar ages and weights (birthdates confirmed).

SMCM MRI Demonstrates Delayed Clearance Correlating with OA Severity

SMCM was used to characterize inflow and outflow parameters of bone circulation. Perfusion in OA subchondral bone is characterized in the TIC by a lack of clearance with increasing severity of OA (Figure 1). Pharmacokinetic analysis of the DCE-MRI data demonstrated that the clearance or washout rate of the contrast agent (k^{el}) in the medial tibial plateau decreased with increasing severity of OA (Mankin score) indicative of outflow obstruction and venous stasis ($R^2=0.54$, $p=0.015$) (Figure 2). No differences were observed in other pharmacokinetic parameters, in either the medial or lateral tibial plateaus.

MMCM MRI Demonstrates Reduced Permeability Surface Area in Severe OA

MMCM was used to examine the degree of capillary permeability to verify that signal enhancement was due to flow characteristics and not to accumulation of the contrat agent in

the intraosseous, extravascular space. Measurement of the permeability surface area product (PS) in the medial tibial plateau did not demonstrate an increase in capillary permeability. In fact, a moderate decrease in PS with increasing OA severity was observed (R^2=0.50, p=0.048). Together with non-significant plasma volume and fractional leak rate, these data suggest that the signal enhancement observed with SMCM was not due to increased capillary permeability and transvascular migration of contrast agent into the intrasosseous extravascular space.

PET Analysis for Decreased Perfusion, Blood Volume, and Bone Uptake

Incorporation of ^{18}F-Fluoride was used to measure both perfusion and its relationship to incorporation of the isotope into bone matrix. Asymmetric radiotracer uptake, with decreased uptake in areas of severe OA, was observed (Figures 3, 4). Time activity curves (TAC) were created to quantify ^{18}F-Fluoride uptake in specific anatomic regions. At 2 minutes after injection, perfusion in the medial tibial compartment with OA is approximately two-thirds that of the lateral tibial compartment without OA (Figure 5, arrow). A 3 compartment pharmacokinetic fit of the ^{18}F-Fluoride TAC was used to model bone blood flow (K^1), blood volume (V^b), and net ^{18}F-Fluoride influx rate (K^i). The blood volume (V^b) decreased with increasing severity of cartilage lesions in the medial tibial plateau (R^2=0.64, p=0.005) (Figure 6a). A decrease in bone blood flow (K^1) in the medial tibial plateau was observed with increasing severity of OA (R^2=0.52, p = 0.019) (Figure 6b). Influx rates of tracer (K^i), in the bone decreased with increasing OA severity on the medial side (R^2=0.40, p = 0.05) (Figure 6c). A significant correlation was found between blood flow (K^1) and the net tracer influx rate (K^i) in the medial tibial bone (R^2=0.95; p<0.001) compared to a much lesser correlation on the lateral side (R^2=0.58; p=0.01) (Figure 6d).

Histology and Histomorphometry

Quantitative histomorphometric parameters were compared in the medial tibial subchondral trabecular bone between knees with mild cartilage lesions (Mankin scores 1-6), and severe cartilage lesions (Mankin scores 12-14). The percent trabecular bone area was 59.2±8.4% in mild OA compared to 44.4±4.5% in severe OA (p=0.01), indicating relative osteopenia in the trabecular bone subjacent to more severe cartilage lesions. Invasion of the subchondral bone plate and calcification of cartilage precluded accurate quantification of subchondral bone plate thickness. The subchondral trabecular thickness and separation were not significantly different in mild and severe OA. Martius blue staining demonstrated no intraosseous thrombi in either group (Figure 7). Thrombomodulin produces an anticoagulant endothelial surface and loss of endothelial thrombomodulin staining has been linked to hypercoagulability and local thrombosis. Thrombomodulin staining was positive in the endothelium indicating a non-thrombogenic endothelial surface in all animals (Figure 7 arrows). These observations suggest that the outflow obstruction observed with DCE-MRI was not associated with intraosseous vascular occlusion.

Discussion

Modeling the relationships derived from DCE-MRI TICs demonstrates a prolonged increase in signal intensity during the clearance or washout phase and a decrease in the elimination

constant, k^{el}, of SMCM Gd-DTPA with OA of increasing severity. Other perfusion parameters derived from TICs are unchanged. Delayed contrast clearance was observed only on the medial side coincident with the severity of OA. Relatively normal bone in the unaffected lateral tibial plateau exhibited normal contrast clearance. These results are consistent with our previous observations describing outflow obstruction in younger guinea pigs even before cartilage lesions appear, and with other subsequent observations with DCE-MRI.[15; 30] Analysis of the TICs of the MMCM uptake showed no increase in the permeability surface area product (PS) with increasing severity of OA, suggesting that the increased signal intensity observed in OA is probably not due to increased permeability and transvascular migration of Gd-DTPA to the intraosseous extravascular space. A recent study also demonstrated a decrease in the DCE-MRI plasma elimination constant, k^{el}, in subjects with reduced bone mineral density and decreased percent bone area in tibial plateaus with severe OA and osteoporosis.[17]

The elevated signal enhancement patterns seen on DCE-MRI during the clearance phase suggest the presence of venous outflow obstruction and venous stasis. Previously, intraosseous venography has demonstrated markedly delayed venous drainage and occlusion of retinacular veins in OA of the hip with drainage of the proximal femur through diaphyseal intramedullary veins.[13] In physiologic and anatomic studies of established human OA, circulatory alterations consisting of decreased venous drainage, venous outflow obstruction, and venous stasis have been reported, associated with intraosseous hypertension, reductions in perfusion, and relative hypoxia.[13; 31] Together, the present functional study and previous physiologic and anatomic studies strongly suggest venous outflow obstruction, venous stasis and a “venous outlet syndrome” with reduced perfusion and hypoxia as a pathophysiologic mechanism in OA.[9; 12-14; 32]

We observed no intraosseous thrombi and vessels maintained a non-thrombogenic endothelial membrane suggesting that mechanisms other than intraosseous thrombotic occlusion are responsible for decreased clearance of contrast agent. Several mechanisms exist that could suggest a *functional*, rather than *structural*, increase in venous outflow resistance. Venous stasis could have been produced by increased intraosseous extravascular pressure or extraosseous venous shunting, both of which have been demonstrated in OA.[12; 13; 32] Bone venous vasculature is relatively more sensitive to vasoconstricting agents and are responsive to a number of cytokines resident in bone particularly endothelin, a vasoconstricting agent that is released from endothelial cells by hypoxia.[33; 34]

The PET data confirm that decreased perfusion is related to the severity of OA and extends that observation to show a relationship between changes in the circulatory environment in subchondral bone (decreased perfusion) and abnormal bone metabolism (decreased ^{18}F-Fluoride influx) associated with the severity of OA. Using compartmental modeling of ^{18}F-Fluoride, TACs of the tibial plateaus exhibit an asymmetric decrease in perfusion and radionuclide incorporation into bone matrix in knees with severe cartilage degeneration. Specifically, we observed in the medial tibial plateau: 1.) A decrease in blood volume and blood flow with increasing cartilage degeneration; 2.) A decrease in radionuclide incorporation into bone matrix with increasing OA, reflecting decreased bone formation consistent with the decrease in percent bone area; and 3.) A strong correlation between

blood flow and ^{18}F-Fluoride incorporation into bone matrix. These observations establish relationships among bone blood flow (K^1), ^{18}F-Fluoride influx rate (K^i), and cartilage lesions in OA. Several previous studies have also demonstrated relationships between K^1 and K^i and support our observations that decreased perfusion is associated with decreased K^i and decreased percent bone area in OA. In one study of normal porcine bone, ^{18}F-Fluoride was incorporated in proportion to bone blood flow demonstrating that blood flow is related to bone formation (R^2=0.74; p<0.001).[27] In a second study, K^i was correlated with bone blood flow (^{15}O-H^2O) following total hip arthroplasty and bone grafting.[28]. A significant correlation has been established between K^i and the mineral apposition rate in porcine bone.[19] While ^{18}F-Fluoride uptake may occur passively, increased uptake and bone formation occur with increased perfusion.[22] A study in human subjects established a correlation of K^i with histomorphometric and biochemical indicators of bone formation.[20] These observations collectively express the relationships of bone blood flow, and kinetic indices of bone formation.[21]

This study indicates that imaging with DCE-MRI and ^{18}F-PET can be used to detect changes in regional perfusion in OA. Pharmacokinetic modeling can be used to estimate kinetic parameters of blood flow including arterial inflow, capillary permeability, and venous outflow, and to correlate circulatory observations with subchondral bone metabolism and structure of interest to the pathophysiology of OA. While speculative, given the known responsiveness of osteoblasts to their physicochemical environment, including flow, pressure, and hypoxia, the significance of the circulatory changes in OA may lie in alterations induced in the osteoblast expression of cytokines that are related to bone remodeling and cartilage breakdown. This study puts previous vascular studies into a functional pathophysiological context and suggests that additional work is needed on perfusion as a contributor to the pathophysiology of OA.[9]

Acknowledgments

The authors acknowledge Dr. Stephen Doty for histomorphometry and Ms. Carol Mackay for histochemistry and immunohistochemistry. The authors acknowledge support of AstraZeneca, U.K. R.K.A. acknowledges support from NIH AR 2K24AR002128-09.

REFERENCES

1. Karsdal MA, Leeming DJ, Dam EB, et al. Should subchondral bone turnover be targeted when treating osteoarthritis? Osteoarthritis Cartilage. 2008; 16:638–646. [PubMed: 18362080]
2. Mansell J, Collins C, Bailey AJ. Bone, not cartilage, should be the major focus in osteoarthritis. Nature clinical practice Rheumatology. 2007; 3:306–307.
3. Quasnichka HL, Anderson-MacKenzie JM, Bailey AJ. Subchondral bone and ligament changes precede cartilage degradation in guinea pig osteoarthritis. Biorheology. 2006; 43:389–397. [PubMed: 16912411]
4. Pastoureau P, Leduc S, Chomel A, et al. Quantitative assessment of articular cartilage and subchondral bone histology in the meniscectomized guinea pig model of OA. OAC. 2003:412–423.
5. Sanchez C, Deberg M, Piccardi N, et al. Subchondral bone osteoblasts induce phenotypic changes in human osteoarthritic chondrocytes. Osteoarthritis Cartilage. 2005; 13:988–997. [PubMed: 16168681]

6. Sanchez C, Deberg MA, Piccardi N, et al. Osteoblasts from the sclerotic subchondral bone downregulate aggrecan but upregulate metalloproteinases expression by chondrocytes. Osteoarthritis Cartilage. 2005; 13:979–987. [PubMed: 16243232]
7. Lyons TJ, McClure SF, Stoddart RW, et al. The normal human chondro-osseous junctional region: evidence for contact of uncalcified cartilage with subchondral bone and marrow spaces. BMC musculoskeletal disorders. 2006; 7:52. [PubMed: 16787529]
8. Arkill KP, Winlove CP. Solute transport in the deep and calcified zones of articular cartilage. Osteoarthritis Cartilage. 2008; 16:708–714. [PubMed: 18023368]
9. Watt I. Osteoarthritis revisited---again! Skeletal Radiol. 2009; 38:419–423. [PubMed: 19183989]
10. Warren SM, Steinbrech DS, Mehrara BJ, et al. Hypoxia regulates osteoblast gene expression. J Surg Res. 2001; 99:147–155. [PubMed: 11421617]
11. Hillsley MV, Frangos JA. Bone tissue engineering: the role of interstitial fluid flow. Biotechnology and bioengineering. 1994; 43:573–581. [PubMed: 11540959]
12. Kiaer T, Pedersen N, Kristensen KD, et al. Intra-osseous pressure and oxygen tension in avascular necrosis and osteoarthritis of the hip. J Bone Joint Surg Br. 1990; 72:1023–1030. [PubMed: 2246284]
13. Arnoldi CC. Vascular aspects of degenerative joint disorders. A synthesis. Acta Orthop Scand Suppl. 1994; 261:1–82. [PubMed: 7976304]
14. Kiaer T, Gronlund J, Sorensen KH. Subchondral pO2, pCO2, pressure, pH, and lactate in human osteoarthritis of the hip. Clin Orthop Relat Res. 1988:149–155. [PubMed: 3127099]
15. Lee J, Dyke J, Ballon D, et al. Subchondral fluid dynamics in a model of osteoarthritis: use of dynamic contrast-enhanced MRI. Osteoarthritis Cartilage. 2009; 17:1350–1355. [PubMed: 19409292]
16. Aaron RK, Dyke JP, Ciombor DM, et al. Perfusion abnormalities in subchondral bone associated with marrow edema, osteoarthritis, and avascular necrosis. Ann N Y Acad Sci. 2007; 1117:124–137. [PubMed: 18056039]
17. Ma HT, Griffith JF, Yeung DK, et al. Modified Brix model analysis of bone perfusion in subjects of varying bone mineral density. J Magn Reson Imaging. 2010; 31:1169–1175. [PubMed: 20432353]
18. Dyke JP, Aaron RK. Noninvasive methods of measuring bone blood perfusion. Ann N Y Acad Sci. 2010; 1192:95–102. [PubMed: 20392223]
19. Piert M, Zittel TT, Becker GA, et al. Assessment of porcine bone metabolism by dynamic [18F]-Fluoride ION PET: Correlation with Bone Histomorphometry. J Nucl Med. 2001; 42:1091–1100. [PubMed: 11438633]
20. Messa C, Goodman W, Hoh CK, et al. Bone metabolic activity measured with positron emission tomography and [18F]fluoride ion in renal osteodystrophy: correlation with bone histomorphometry. The Journal of clinical endocrinology and metabolism. 1993; 77:949–955. [PubMed: 8408470]
21. Frost ML, Siddique M, Blake GM, et al. Differential effects of teriparatide on regional bone formation using 18F-fluoride positron emission tomography. J Bone Miner Res. 2011; 26:1002–1011. [PubMed: 21542003]
22. Doot RK, Muzi M, Peterson LM, et al. Kinetic analysis of 18F-fluoride PET images of breast cancer bone metastases. J Nucl Med. 2010; 51:521–527. [PubMed: 20237040]
23. Brix G, Semmler W, Port R, et al. Pharmacokinetic parameters in CNS Gd-DTPA enhanced MR imaging. J Comput Assist Tomogr. 1991; 15:621–628. [PubMed: 2061479]
24. Tofts PS, Brix G, Buckley DL, et al. Estimating kinetic parameters from dynamic contrast-enhanced T(1)-weighted MRI of a diffusable tracer: standardized quantities and symbols. J Magn Reson Imaging. 1999; 10:223–232. [PubMed: 10508281]
25. van Dijke C, Peterfy C, Brasch R, et al. MRI of the arthritic rabbit knee joint using albumin-(Gd-DTPA)30 with correlation to histopathology. Magn Reson Imaging. 1999; 17:237–245. [PubMed: 10215479]
26. Hawkins RA, Choi Y, Huang SC, et al. Evaluation of the skeletal kinetics of fluorine-18-fluoride ion with PET. J Nucl Med. 1992; 33:633–642. [PubMed: 1569473]

27. Piert M, Zittel TT, Machulla HJ, et al. Blood flow measurements with [(15)O]H2O and [18F]fluoride ion PET in porcine vertebrae. J Bone Miner Res. 1998; 13:1328–1336. [PubMed: 9718202]

28. Temmerman OP, Raijmakers PG, Heyligers IC, et al. Bone metabolism after total hip revision surgery with impacted grafting: evaluation using H2 15O and [18F]fluoride PET; a pilot study. Molecular imaging and biology : MIB : the official publication of the Academy of Molecular Imaging. 2008; 10:288–293. [PubMed: 18543040]

29. Mankin HJ, Dorfman H, Lippiello L, et al. Biochemical and metabolic abnormalities in articular cartilage from osteo-arthritic human hips. II. Correlation of morphology with biochemical and metabolic data. J Bone Joint Surg Am. 1971; 53:523–537. [PubMed: 5580011]

30. Wang YX, Griffith JF, Deng M, et al. Compromised perfusion in femoral head in normal rats: distinctive perfusion MRI evidence of contrast washout delay. The British journal of radiology. 2012; 85:e436–441. [PubMed: 22167506]

31. Kiaer T, Dahl B, Lausten G. Partial pressures of oxygen and carbon dioxide in bone and their correlation with bone-blood flow: effect of decreased arterial supply and venous congestion on intraosseous oxygen and carbon dioxide in an animal model. J Orthop Res. 1992; 10:807–812. [PubMed: 1403294]

32. Pedersen NW, Kiaer T, Kristensen KD, et al. Intraosseous pressure, oxygenation, and histology in arthrosis and osteonecrosis of the hip. Acta Orthop Scand. 1989; 60:415–417. [PubMed: 2816318]

33. Briggs PJ, Moran CG, Wood MB. Actions of endothelin-1, 2, and 3 in the microvasculature of bone. J Orthop Res. 1998; 16:340–347. [PubMed: 9671929]

34. Brinker MR, Lippton HL, Cook SD, et al. Pharmacological regulation of the circulation of bone. J Bone Joint Surg Am. 1990; 72:964–975. [PubMed: 2166739]

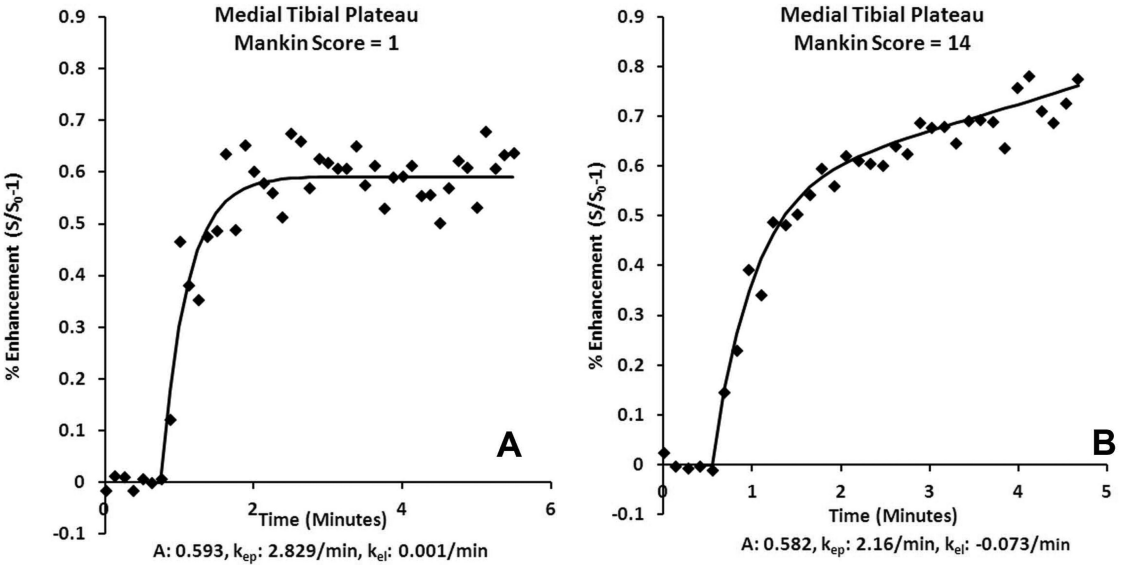

Fig. 1.

SMCM TIC of the medial tibia demonstrating (A) venous contrast clearance in an animal with Mankin score of 0, (B) delayed contrast clearance in an animal with Mankin score of 14.

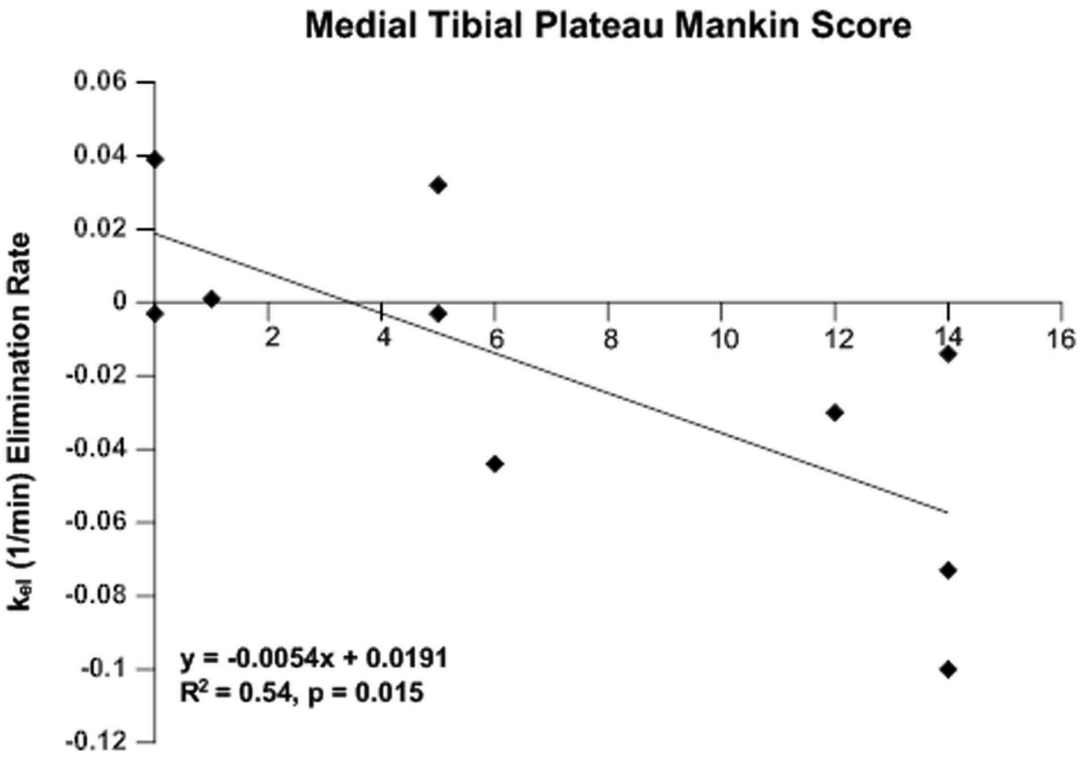

Fig. 2.

SMCM elimination of the subchondral bone with increasing OA. The contrast elimination constant, K^{el}, of the medial tibia decreased with increasing Mankin scores.

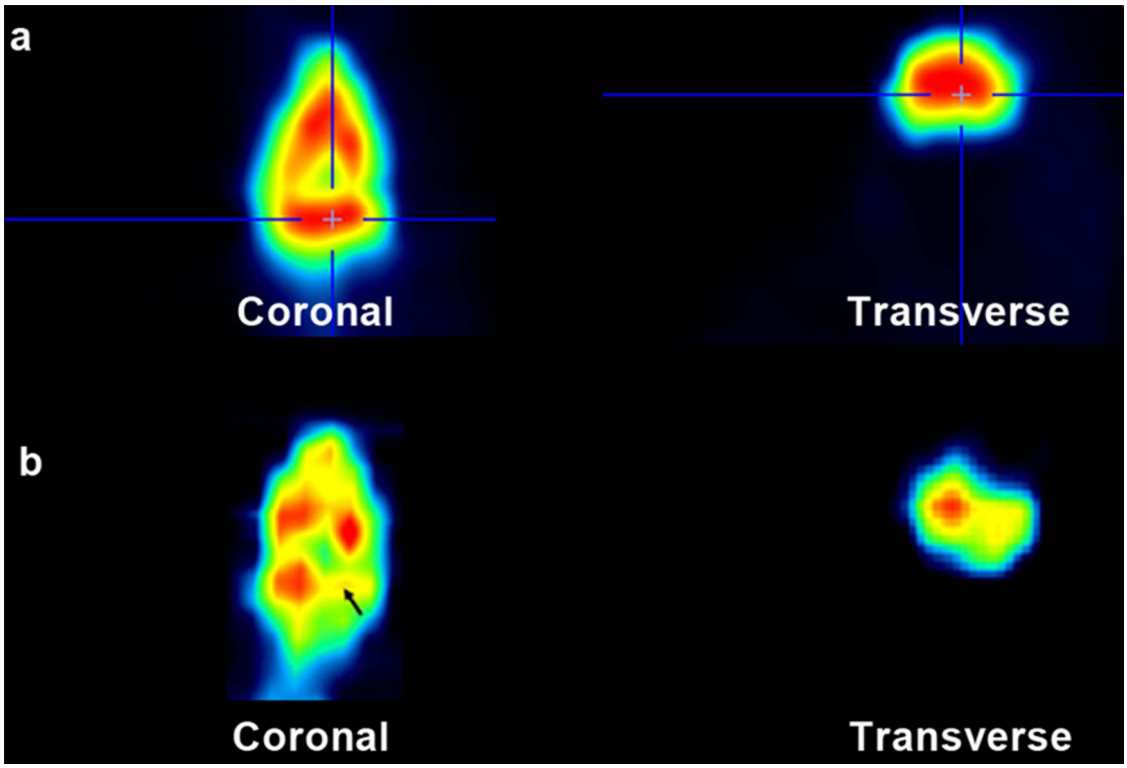

Fig. 3.

False color imaging comparing ^{18}F-Fluoride incorporation in mild and severe OA. Red are areas of high flow; yellow are areas of decreased flow. (a) Symmetrical ^{18}F uptake in mild OA in both medial and lateral tibial plateaus. (b) Uptake is decreased at the site of severe OA in the medial tibial plateau (arrow).

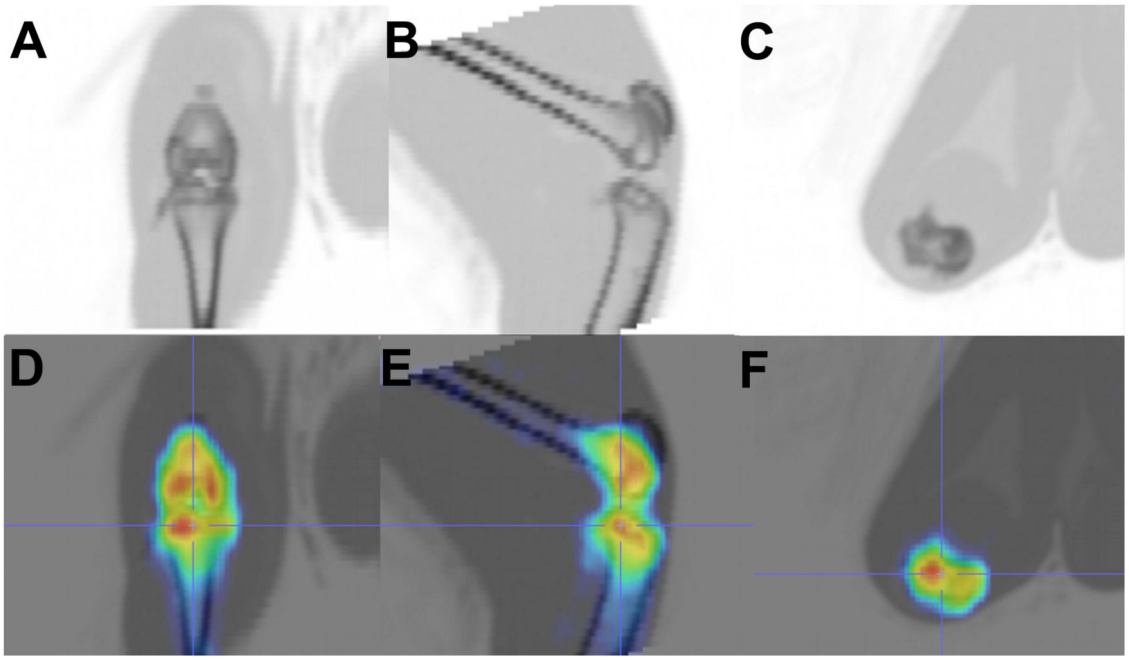

Fig. 4.

CT images of the guinea pig knee. (a.) coronal, (b) sagittal, and (c) transverse views. PET/CT showing anatomic localization of false color images reflecting radionuclide uptake. (d) coronal, (e) sagittal, and (f) transverse views.

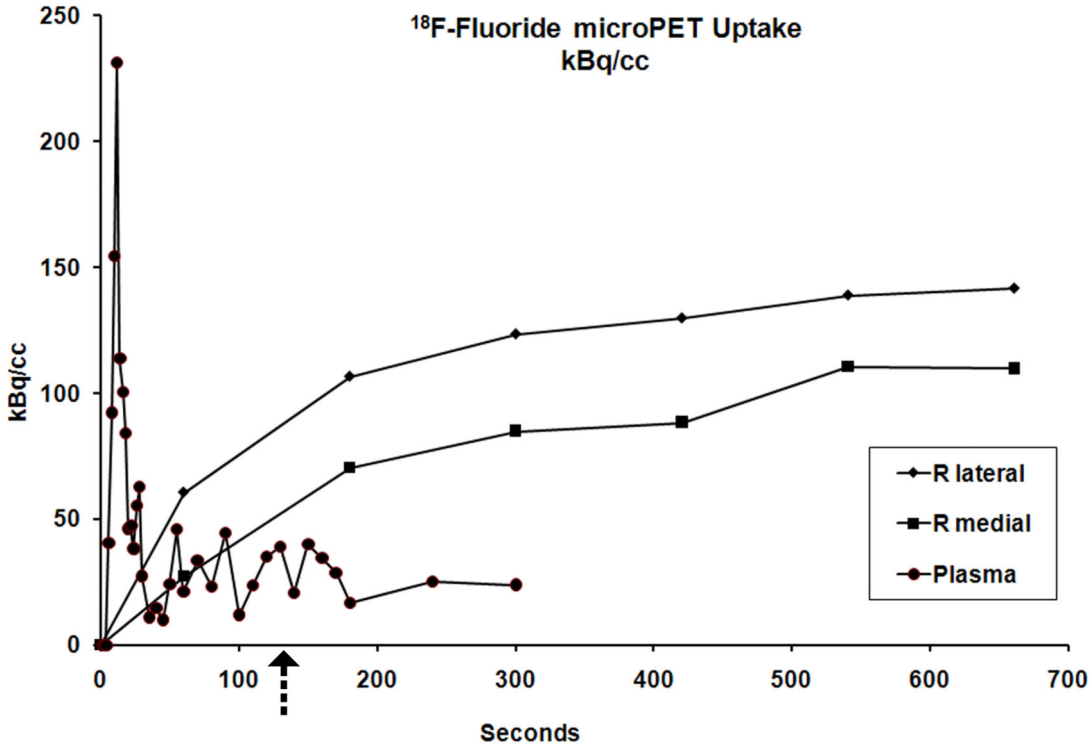

Fig. 5.

Time-activity curve. At 2 minutes after injection (arrow), ^{18}F uptake reflects perfusion. Over the next 45-60 minutes, the ^{18}F becomes progressively incorporated into hydroxyapatite. The arterial input function was sampled by placing an ROI on the femoral artery.

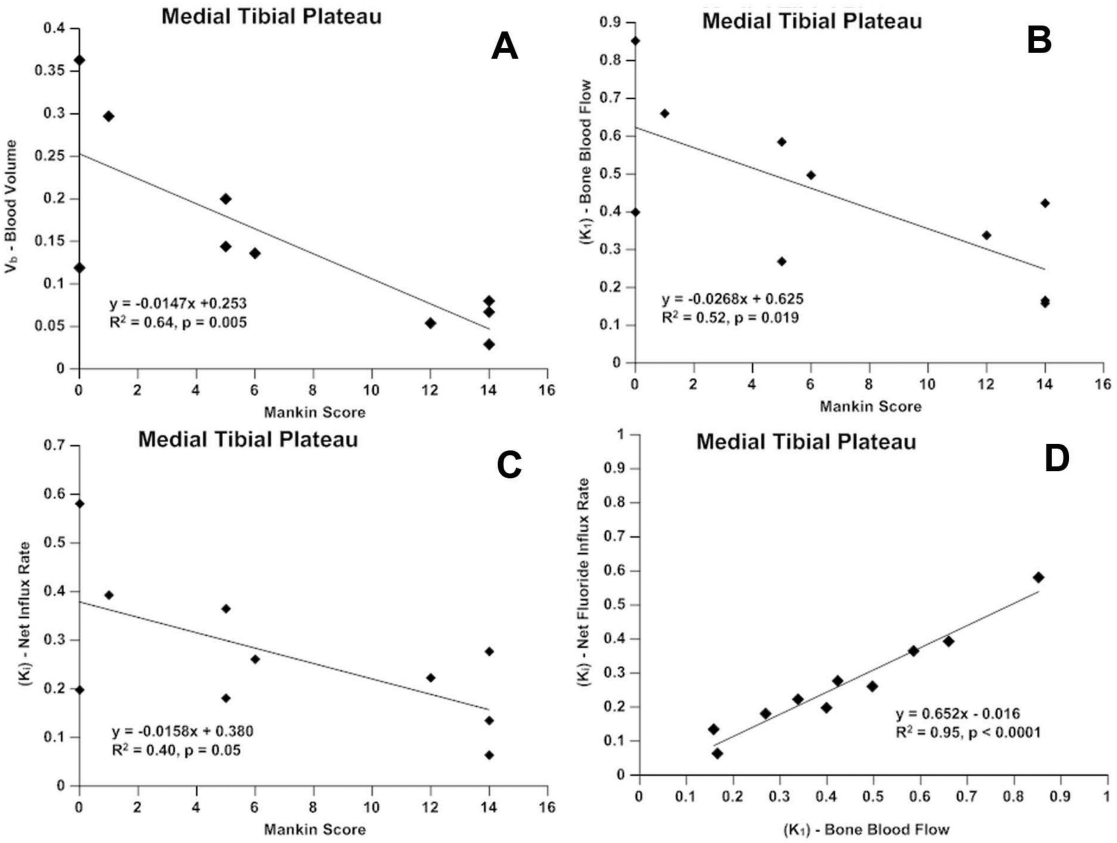

Fig. 6.

PET in the medial tibia. a.) blood volume is reduced with increasing severity of OA; b.) bone blood flow (K^1) decreases with OA severity: c.) net Fluoride influx rate (Ki) decreases with severity of OA: d.) bone blood flow correlates strongly with net Fluoride influx rate.

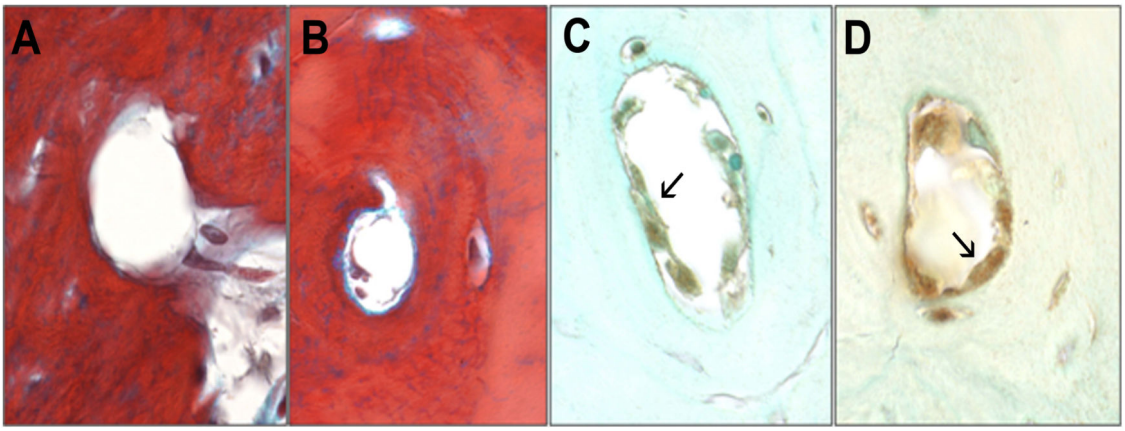

Fig. 7.

Intraosseous vasculature. Martius blue staining for thrombi demonstrated patency of vessels with both normal (A) and delayed (B) contrast clearance. Immunostaining was positive for thrombomodulin in endothelial cells with of both normal (C) and delayed (D) contrast clearance (arrows).